



1-28-2011

## A size-dependent nanoscale metal–insulator transition in random materials

Albert B.K. Chen

*University of Pennsylvania*, [albertbk@seas.upenn.edu](mailto:albertbk@seas.upenn.edu)

Soo Gil Kim

*University of Pennsylvania*

Yudi Wang

*University of Pennsylvania*, [wangyudi@seas.upenn.edu](mailto:wangyudi@seas.upenn.edu)

Wei-Shao Tung

*University of Pennsylvania*, [tungwei@seas.upenn.edu](mailto:tungwei@seas.upenn.edu)

I-Wei Chen

*University of Pennsylvania*, [iweichen@seas.upenn.edu](mailto:iweichen@seas.upenn.edu)

Follow this and additional works at: [https://repository.upenn.edu/mse\\_papers](https://repository.upenn.edu/mse_papers)

 Part of the [Materials Science and Engineering Commons](#)

---

### Recommended Citation

Chen, A. B., Kim, S., Wang, Y., Tung, W., & Chen, I. (2011). A size-dependent nanoscale metal–insulator transition in random materials. Retrieved from [https://repository.upenn.edu/mse\\_papers/215](https://repository.upenn.edu/mse_papers/215)

Postprint version.

Suggested Citation:

Chen, A.B.K., Kim, S.G., Wang, Y., Tung, W. and Chen, I. (2011). A size-dependent nanoscale metal–insulator transition in random materials *Nature Nanotechnology*, Vol. 6. pp. 237-241.

Publisher URL: <http://dx.doi.org/10.1038/nnano.2011.21>

This paper is posted at ScholarlyCommons. [https://repository.upenn.edu/mse\\_papers/215](https://repository.upenn.edu/mse_papers/215)  
For more information, please contact [repository@pobox.upenn.edu](mailto:repository@pobox.upenn.edu).

---

## A size-dependent nanoscale metal–insulator transition in random materials

### Abstract

Insulators and conductors with periodic structures can be readily distinguished, because they have different band structures, but the differences between insulators and conductors with random structures are more subtle. In 1958, Anderson provided a straightforward criterion for distinguishing between random insulators and conductors, based on the 'diffusion' distance  $\zeta$  for electrons at 0 K (ref. 3). Insulators have a finite  $\zeta$ , but conductors have an infinite  $\zeta$ . Aided by a scaling argument, this concept can explain many phenomena in disordered electronic systems, such as the fact that the electrical resistivity of 'dirty' metals always increases as the temperature approaches 0 K (refs 4–6). Further verification for this model has come from experiments that measure how the properties of macroscopic samples vary with changes in temperature, pressure, impurity concentration and applied magnetic field, but, surprisingly, there have been no attempts to engineer a metal–insulator transition by making the sample size less than or more than  $\zeta$ . Here, we report such an engineered transition using six different thin-film systems: two are glasses that contain dispersed platinum atoms, and four are single crystals of perovskite that contain minor conducting components. With a sample size comparable to  $\zeta$ , transitions can be triggered by using an electric field or ultraviolet radiation to tune  $\zeta$  through the injection and extraction of electrons. It would seem possible to take advantage of this nanometallicity in applications.

### Disciplines

Engineering | Materials Science and Engineering

### Comments

Postprint version.

### Suggested Citation:

Chen, A.B.K., Kim, S.G., Wang, Y. Tung, W. and Chen, I. (2011). A size-dependent nanoscale metal–insulator transition in random materials *Nature Nanotechnology*, Vol. 6. pp. 237-241.

Publisher URL: <http://dx.doi.org/10.1038/nnano.2011.21>

# A size-dependent nanoscale metal-insulator transition in random materials

Albert B. K. Chen<sup>†</sup>, Soo Gil Kim<sup>†</sup>, Yudi Wang<sup>†</sup>, Wei-Shao Tung and I-Wei Chen<sup>\*</sup>

**1 Insulators and conductors with periodic structures can be**  
**2 readily distinguished, because they have different band struc-**  
**3 tures, but the differences between insulators and conductors**  
**4 with random structures are more subtle<sup>1,2</sup>. In 1958, Anderson**  
**5 provided a straightforward criterion for distinguishing**  
**6 between random insulators and conductors, based on the 'diffu-**  
**7 sion' distance  $\zeta$  for electrons at 0 K (ref. 3). Insulators have a**  
**8 finite  $\zeta$ , but conductors have an infinite  $\zeta$ . Aided by a scaling**  
**9 argument, this concept can explain many phenomena in disor-**  
**10 dered electronic systems, such as the fact that the electrical**  
**11 resistivity of 'dirty' metals always increases as the temperature**  
**12 approaches 0 K (refs 4–6). Further verification for this model**  
**13 has come from experiments that measure how the properties**  
**14 of macroscopic samples vary with changes in temperature,**  
**15 pressure, impurity concentration and applied magnetic**  
**16 field<sup>4,5</sup>, but, surprisingly, there have been no attempts to engin-**  
**17 eer a metal-insulator transition by making the sample size less**  
**18 than or more than  $\zeta$ . Here, we report such an engineered tran-**  
**19 sition using six different thin-film systems: two are glasses that**  
**20 contain dispersed platinum atoms, and four are single crystals**  
**21 of perovskite that contain minor conducting components. With**  
**22 a sample size comparable to  $\zeta$ , transitions can be triggered by**  
**23 using an electric field or ultraviolet radiation to tune  $\zeta$  through**  
**24 the injection and extraction of electrons. It would seem possible**  
**25 to take advantage of this nanometallicity in applications.**

26 We studied nominally insulating thin films that had a random  
 27 composition (perovskite crystals) or an outright amorphous struc-  
 28 ture (glasses) and included minor conducting components. To  
 29 unambiguously distinguish a size-triggered metal-insulator tran-  
 30 sition (MIT) from conventional percolation<sup>6</sup>, in which conductivity  
 31 persists over a macroscopic length scale, we focused on compo-  
 32 sitions with a conducting fraction  $f$  well below the bulk percolation  
 33 limits (these are listed for several systems in Table 1). Aiming at a  
 34 nanoscale  $\zeta$ , we probed  $\zeta$  in films of various nanoscale thickness  
 35  $\delta$ : films with  $\delta \ll \zeta$  are metallic across the thickness, films  
 36 with  $\delta \gg \zeta$  are insulating. We also examined films with  $\delta \approx \zeta$  to  
 37 attempt an externally stimulated MIT. All the films studied had  
 38 macroscopic lateral sizes, so laterally they were insulating.

39 Our first example was amorphous SiO<sub>2</sub> doped with Pt atoms  
 40 finely dispersed at the scale of <0.5 nm (the transmission electron  
 41 micrograph and corresponding electron diffraction are shown in  
 42 the insets of Fig. 1a,b, respectively). The lateral percolation limit  
 43 was  $f \approx 0.38$  (molar fraction of Pt in SiO<sub>2</sub>:Pt); above this the sheet  
 44 resistance (per four-point probe) decreased with decreasing temp-  
 45 erature  $T$ , and below it, the opposite held (Supplementary  
 46 Fig. S1). At  $f \geq 0.33$ , the UV reflectivity shows a peak at 270 nm  
 47 (Fig. 1), which is the plasmon resonance of metallic Pt nanoparticles  
 48 in SiO<sub>2</sub>; this signature resonance is also commonly used to charac-  
 49 terize dispersed nanoparticles of Au and Ag of dilute concen-  
 50 trations<sup>7</sup>. There is no such peak at  $f = 0.2$ , suggesting the absence

of metallic clusters. Despite the lack of metallic clusters, evidence  
 for free carriers at  $f = 0.2$  appeared in the long-wavelength  
 (>15  $\mu\text{m}$ ) optical data under the characteristic SiO<sub>2</sub> vibration  
 peak (Fig. 1b). At increasing wavelengths, there is an increasing  
 reflectivity background that can be fitted by Drude's formula for dis-  
 sipative conducting electrons<sup>8</sup>. The fitted plasma energy is  
 $\sim 0.068$  eV, corresponding to a carrier (assuming free electron) con-  
 centration of  $8.4 \times 10^{16} \text{ cm}^{-3}$ . The concentration increased to  
 $1.47 \times 10^{17} \text{ cm}^{-3}$  at  $f = 0.29$ . Therefore, in these SiO<sub>2</sub>:Pt glasses,  
 we have found a material that is macroscopically insulating, but  
 (infrared) optically conducting, which fits Anderson's picture of a  
 random insulator with a finite  $\zeta$ .

We expect a  $\delta \ll \zeta$  film to be an ohmic conductor and a  $\delta \gg \zeta$   
 one to be a non-ohmic insulator, so resistance-voltage testing  
 across the film thickness (Fig. 2a) offers a way to determine  $\zeta$ . For  
 $f = 0.2$ , the virgin film was ohmic up to  $\delta = 16$  nm. At 21 nm, it  
 was non-ohmic with a high resistance. Here, a positive voltage  $V$   
 refers to having a current  $I$  flowing across a test cell from top to  
 bottom, with a resistance  $R = V/I$ . This would suggest  $16 \text{ nm} <$   
 $\zeta < 21 \text{ nm}$ . However, we also found that films with thicknesses  
 from 7 nm to 16 nm underwent a voltage-induced MIT: a  $R$ - $V$  hys-  
 teresis between two resistance states (HR, high resistance; LR, low  
 resistance) switching at a certain sharp 'set' voltage  $V_{\text{set}}$  from LR  
 to HR, then reversing at several step-like 'reset' voltages  $V_{\text{reset}}$ . The  
 HR state of the 16 nm film (broken curve in Fig. 2a) was particularly  
 precarious, varying from run to run and from cell to cell. In contrast,  
 the thicker film (21 nm) in Fig. 2a (for  $f = 0.2$ ) had a stable high  
 resistance that did not switch, whereas a film of a similar thickness  
 (20 nm) but higher  $f$  had an ohmic low resistance in the virgin state,  
 then switched at about the same voltage (Fig. 2c). These results are  
 summarized in the  $\delta$ - $f$  map in Fig. 2b, which delineates a relatively  
 wide window for voltage-induced MIT. Such data allow us to define

**Table 1 | Nanometallic thin films with  $\zeta \approx 20$  nm.**

Solid solutions	$f_c$ (mol%)	$V_{\text{set}}$ (eV)	Predicted FNT barrier (eV)	$f_{\text{percolation}}$ (mol%)
CZO-SRO	5.5	2.2	2.5	75
LAO-SRO	11	2.2	2.5	86
CZO-LNO	25	2.2	2.5	-
LAO-LNO	12	2.2	2.5	-
SiO <sub>2</sub> -Pt	29	4.2	4.1	38
SiN <sub>4/3</sub> -Pt	25	3.0	2.9	38

For Si<sub>3</sub>N<sub>4</sub>:Pt,  $\zeta \approx 25$  nm. Values of  $f_c$  (in mol% of conductor) are insensitive to electrode material (Pt, Au, SRO, Mo, Ag, and Ta, in the order of decreasing work function) and substrate orientation (001, 011 and 111 STO for perovskites and 100 and 110 Si for amorphous solutions of SiO<sub>2</sub>:Pt and Si<sub>3</sub>N<sub>4</sub>:Pt). Values of  $V_{\text{set}}$  (top electrode, Pt; bottom electrode, SRO) are in agreement with the predicted Fowler-Nordheim tunnelling barrier from the highest occupied state of the less noble electrode (SRO) to the lowest unoccupied state of the insulator. Electron tunnelling at  $V_{\text{set}}$  is directed from the less noble electrode to the more noble electrode (see Supplementary Figs S2, S3 and S7 and Table S1 for details). The bulk percolation limits are estimates from the macroscopic MIT data summarized in Supplementary Section A.

Department of Materials Science & Engineering, University of Pennsylvania, Philadelphia, Pennsylvania 19104, USA; <sup>†</sup>These authors contributed equally to this work. \*e-mail: iweichen@seas.upenn.edu

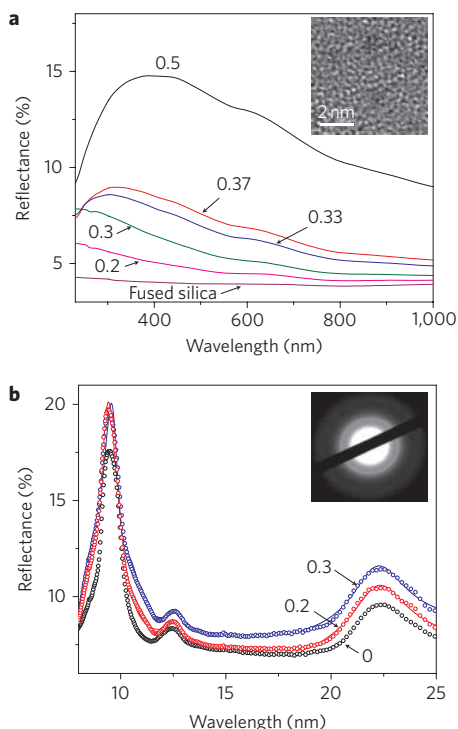


**Figure 1 | Optical evidence of metallic clusters and free carriers.** **a**, UV reflectivity of 40 nm  $\text{SiO}_2$ :Pt films; the peak at 270 nm characteristic of metallic Pt nanoparticles is completely absent at  $f = 0.2$ . Inset: transmission electron micrograph of 12 nm  $\text{SiO}_2$ :0.2 Pt film with a worm-like random structure without apparent segregation. **b**, Infrared reflectivity (200 nm films) featuring, at  $f = 0$ , only the vibrational peaks (at 9.5, 12.5, 22.5 nm) of  $\text{SiO}_2$ , and at  $f > 0$  the same peaks plus a background due to dissipative conducting electrons. Electron contribution increases with wavelength, causing an increase of peak intensity at 22.5 nm with Pt content, in agreement with the Drude model fitting the data (shown as solid curves for  $f = 0.2$  and 0.3). Inset: electron diffraction pattern of 12 nm  $\text{SiO}_2$ :0.2 Pt film with a diffuse ring typical of amorphous material<sup>27</sup>.

1 a statistically more meaningful  $\zeta$  as the mid-point in the window;  $\zeta$   
 2 gradually increases with  $f$ , and suddenly diverges as  $f$  approaches the  
 3 bulk percolation limit.

4 Remarkably, regardless of their locations in the map, all the  
 5 switchable films had a  $V_{\text{set}}$  that was independent of  $f$  and  $\delta$   
 6 (Fig. 2b, inset). This indicates that switching is not field-dependent,

instead having an energetic origin. It is also consistent with its temper-  
 7 ature ( $T$ ) dependence, or lack thereof; at lower  $T$ , the hysteresis  
 8 loop (Fig. 2c) expanded vertically but  $V_{\text{set}}$  remained unchanged.  
 9 This argues against a thermally activated switching mechanism,  
 10 such as ionic/atomic migration or electron hopping. In the litera-  
 11 ture, many insulators have been reported to undergo reversible  
 12 resistance switching triggered by the huge electric field across a  
 13 thin film, which either motivated atomic/ionic motion over a  
 14 distance of several unit cells to form/break conducting filaments or  
 15 charged barrier layers, or enabled redox reactions, especially at elec-  
 16 trode interfaces<sup>9–16</sup>. Recently<sup>15,16</sup>, UV irradiation was found to lower  
 17 the resistance of switchable  $\text{TiO}_2$ /molecular junctions that under-  
 18 went redox reactions (at the external surface), and likewise of  
 19  $\text{Cu}_x\text{O}$  films that contained conducting filaments that were sub-  
 20 sequently broken. This implies that UV irradiation can enable elec-  
 21 tronic switching via the redox mechanism if excess electrons and  
 22 holes are immediately transported away; otherwise, they will rever-  
 23 se/negate the redox reactions. In our film, nanometallicity naturally  
 24 provided this function. This means that the entire film may be able  
 25 to undergo UV-enabled electronic switching by mechanisms that  
 26 must be accompanied by draining of excess electrons or holes.  
 27 Indeed, without applying a voltage, we found UV irradiation was  
 28 able to revive a ‘dead’ cell stuck at the HR after repeated switching  
 29 (Fig. 3a). Clearly, there was no long-range atomic/ionic motion here  
 30 to repair the ‘fatigue’ damage. (Electron trapping/detrapping could  
 31 be one switching mechanism, which can operate under both voltage  
 32 and UV stimulation.)

Parallel observations of nanometallic MIT were made in other  
 34 random materials. One was a  $\text{Si}_3\text{N}_4$  glass similarly doped with Pt,  
 35 the other adopted a lattice construct that was perfectly regular but  
 36 randomized by atomic mixing—a perovskite solid solution made  
 37 into an epitaxial thin film to avoid line and planar defects that  
 38 might have provided electrical shorts<sup>17,18</sup>. These solid solutions  
 39 were hosted by either  $\text{LaAlO}_3$  (LAO) or  $\text{CaZrO}_3$  (CZO), two excel-  
 40 lent insulators, and doped with a small amount of  $\text{LaNiO}_3$  (LNO) or  
 41  $\text{SrRuO}_3$  (SRO), two well-known electronic conductors. Although  
 42 mismatches between cations of different valences and sizes occupy-  
 43 ing the so-called  $A$  site ( $\text{Sr}^{2+} > \text{La}^{3+} > \text{Ca}^{2+}$ ) and the  $B$  site  
 44 ( $\text{Zr}^{4+} > \text{Ru}^{4+} > \text{Ni}^{3+} > \text{Al}^{3+}$ ) could have motivated cation order-  
 45 ing or segregation in these solid solutions, we avoided it by lowering  
 46 the deposition temperature. Therefore, even at a relatively high frac-  
 47 tion such as  $f = 0.25$  in a 3:1 mixture of CZO and LNO, the high-  
 48 resolution cross-sectional image of Fig. 4 and its Fourier transform  
 49 (Fig. 4, inset) revealed only intense diffuse scattering (expected for a  
 50 concentrated random solid solution) and no evidence of ordering or  
 51 phase separation. Their MIT could all be triggered by varying  $\delta$  or  
 52

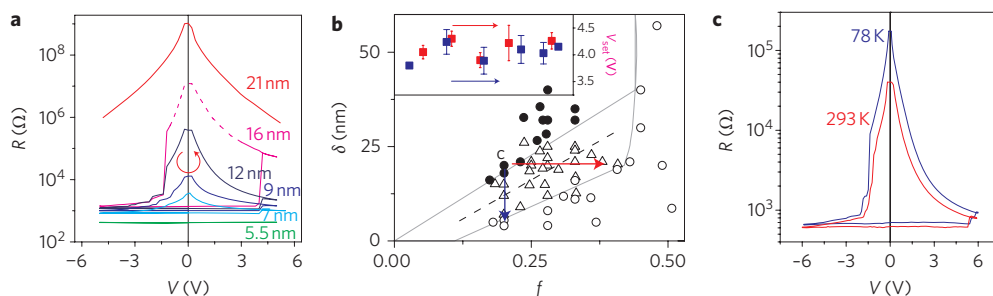


**Figure 2 | R-V dependence on thickness, composition and temperature.** **a**, Cycle from 0 V, to (-) V, to (+) V, to (-) V, to 0 V traces a R-V loop for  $\text{SiO}_2$ :0.2 Pt of various thickness. These are ‘first loops’; that is, samples were not subject to any previous electrical stimulus/forming. When  $\delta \approx \zeta$ , the hysteresis loop provides non-volatile memory. Top electrode, Pt; bottom electrode, Mo. **b**,  $\delta$ - $f$  map for  $\text{SiO}_2$ : $f$  Pt delineating boundaries for conductors (open circles) and insulators (filled circles) separated by switchable films (triangles), abruptly rising at  $f \approx 0.4$  near the bulk percolation limit. Top electrode, Pt; bottom electrode,  $\text{SrRuO}_3$  and Mo (same results). The bisector (broken line) between the boundaries is taken as  $\zeta$ . Inset:  $f$ - $\delta$  independent  $V_{\text{set}}$  for samples along the horizontal red arrow (same  $\delta$ , increasing  $f$ , as red squares) and vertical blue arrow (same  $f$ , decreasing  $\delta$ , as blue squares). **c**, R-V loops at two temperatures for 20 nm  $\text{SiO}_2$ :0.25 Pt. Top electrode, Pt; bottom electrode, Mo. Note that  $f$  in **c** is higher than in **a**.

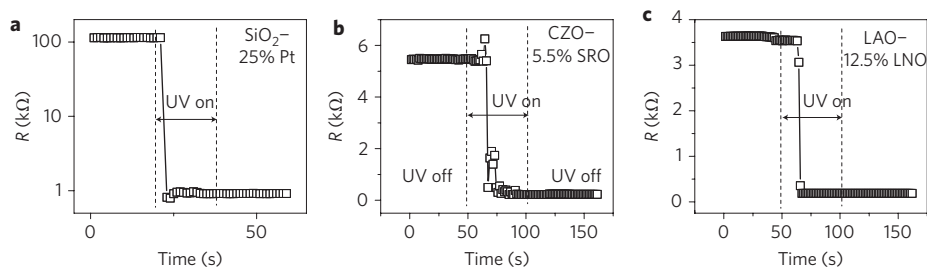


**Figure 3 | UV-triggered HR-to-LR transitions.** **a**, HR of a fatigue-damaged cell promptly decreases when UV is turned on at room temperature. (The low resistance stayed permanently after the light was turned off. The outcome was identical, whether the cell was shorted to the ground or under a small positive/negative bias voltage.) 20 nm SiO<sub>2</sub>:0.25 Pt; top electrode, Pt; bottom electrode, Mo. **b,c**, Further examples of UV-triggered HR-to-LR transitions in CaZrO<sub>3</sub>:0.055 SrRuO<sub>3</sub> (**b**) and LaAlO<sub>3</sub>:0.125 LaNiO<sub>3</sub> (**c**) films. (For other examples see Supplementary Fig. S4.)

the voltage (Supplementary Fig. S2, S3), and their HR-to-LR transition could be rendered by UV irradiation without application of a voltage (Fig. 3b,c).  $\delta$ - $f$  maps similar to the one in Fig. 2b were also observed, as was a  $\delta$ - $f$ - $T$  independent  $V_{\text{set}}$ . Moreover, despite the large differences in structure, chemistry and  $f$  (see Table 1), the traces for their hysteretic loops (Supplementary Fig. S2, S3) all proceeded in the same, anticlockwise manner as in Fig. 2a, provided the top electrode (for example, Pt) had a higher work function than the bottom electrode (for example, SRO). All these observations, common to every nanometallic random material studied here, are supportive of an electronic mechanism.

Despite their similarity, different random materials did have different  $\zeta(f)$  dependence. Table 1 lists the requisite  $f_c$  to render metallicity with  $\zeta \approx 20$  nm. The perovskite data are particularly interesting. First, nanometallicity at low  $f_c$  values is itself remarkable, because the bulk percolation limit in these materials is typically at  $f > 0.7$  (Table 1): a conducting perovskite rapidly loses bulk metallicity with a very modest addition of apparently any insulating perovskite<sup>19</sup>. The very low  $f_c$  of perovskites thus firmly rejects the notion that nanometallicity is due to percolation between metallic nanoparticles. Second, the  $f_c$  of perovskites appears to be correlated to the electron wave function of the cation (more extended for Ru-4d than for Ni-3d in the conducting component) and their valence variation ( $\Delta Z = 0$  for Ru<sup>4+</sup>/Zr<sup>4+</sup> and Ni<sup>3+</sup>/Al<sup>3+</sup>, but not other pairs of B-site cations). The smallest  $f_c$  is required for CZO:SRO (more extended,  $\Delta Z = 0$ ), more for LAO:SRO (more extended,  $\Delta Z \neq 0$ ) and LAO:LNO (less extended,  $\Delta Z = 0$ ), and most for CZO:LNO (less extended,  $\Delta Z \neq 0$ ). This correlation may be used to guide perovskite formulation in engineering nanometallicity in the absence of a detailed knowledge of electronic structure in random materials. Compared to perovskites, the amorphous SiO<sub>2</sub>:Pt and Si<sub>3</sub>N<sub>4</sub>:Pt have more extended Pt-5d electrons but also considerably greater structural and charge disorders, so their  $f_c$  is higher and closer to the bulk percolation limit.

We now compare the LR and HR states with the conventional metallic and insulating states. In Fig. 2c, the rapid decrease of the HR with  $T$  is consistent with an insulating state, but the decrease of LR with  $T$  is too modest for a typical insulator. (Later, in Fig. 5b, we will find that LR can also increase with  $T$ .) Using SRO as the bottom electrode, we show in Supplementary Fig. S6 that the LR was mainly due to the spreading resistance of the bottom electrode: its  $T$  dependence mirrored that of SRO, a ferromagnetic metal, featuring a spin-fluctuation-scattering kink at the Curie temperature (160 K)<sup>20</sup>. Importantly, even with the spreading resistance contribution, the LR remained finite and small as  $T$  approached 0 K. So, LR must be metal-like and cannot be related to electron hopping between impurity states/bands, for which diminishing thermal activation would have caused a divergent resistance toward 0 K (ref. 6). A metallic LR is also consistent with its ohmic  $R(V)$  behaviour, in contrast to the non-ohmic HR.

Because the HR contains only a small contribution from the spreading resistance, we will use it to illustrate some features of nanometallicity. First, the HR does not conform to the Ohm's law of macroscopic resistors. Instead, it follows  $R \approx \exp(\delta/a)$ , with  $a \approx 1.2$  nm being another localization length (Fig. 5a), which is the expected length dependence in the localization regime<sup>4-6</sup>. Therefore, a drastic shortening of  $\zeta$  to some new localization length commensurate with  $a$  occurred at  $V_{\text{set}}$ , thus triggering the MIT. Physically, we suggest that the transition could be due to the injection of electrons, which are trapped at sites near the original conducting pathways; they then erect Coulomb repulsions that 'choke off' further electron passage along the nanometallic pathway. Assuming electron trapping occurs by Fowler-Nordheim tunnelling (FNT)<sup>21</sup> from the nanometallic path to a trap site, through a barrier that is the gap between the highest occupied state of the conductor and the lowest unoccupied state of the insulator, we estimated the required transition voltage as shown in Table 1. This compares well with the observed  $V_{\text{set}}$ .

Under a reverse bias, successive detrapping through the same tunnelling barrier typically leaves behind a series of intermediate states. One such set is shown in Fig. 5b (inset) and interrogated using their small signal  $I$ - $V$ - $T$  curves ( $\pm 0.2$  V). As shown Fig. 5b, their resistances all saturated at low  $T$ . (Note also the LR increase with  $T$  in the bottom curve.) So, again, electron conduction in these states was not thermally activated at sufficiently low temperatures, despite the negative slope of  $R(T)$ . These characteristics are reminiscent of 'bad' metals and can be quantitatively fitted (curves in Fig. 5b) using Sheng's model of fluctuation-induced

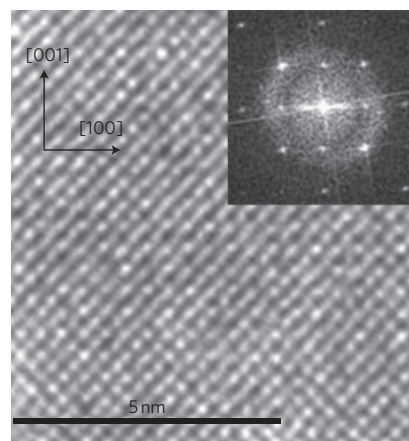


**Figure 4 | Random perovskite solid solution.** Cross-sectional high-resolution TEM image along the [010] direction of a 3:1 mixture of CaZrO<sub>3</sub> and LaNiO<sub>3</sub> film (30 nm) on a 100 SrTiO<sub>3</sub> substrate with a 30 nm buffer of SrRuO<sub>3</sub>. Inset: fast Fourier transform of the same region.

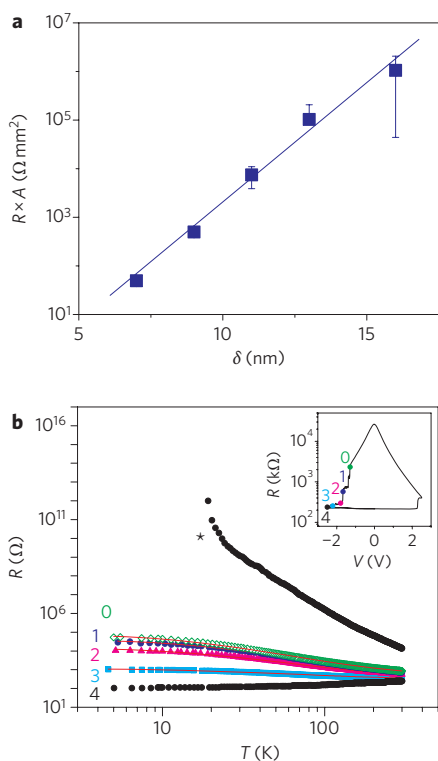


**Figure 5 |  $R$ - $\delta$  and  $R$ - $T$  dependencies.** **a**, HR, multiplied by cell area  $A$ , increases exponentially with film thickness.  $\text{SiO}_2$ :0.25 Pt; top electrode, Pt; bottom electrode, Mo. **b**, Logarithmic temperature dependence of resistance of the LR state (4) and four intermediate states (0–3) shown in the inset. Also shown are data (\*) from another sample with a more resistive HR. Curves 0–3 are model fit using FIT: tunnelling along a metallic channel with one gap of spacing  $\sim 0.4$ – $1.2$  nm and effective gap capacitor area  $\sim (0.2 \text{ nm}^2)$ – $(0.8 \text{ nm}^2)$ .  $\text{LaAlO}_3$ :0.13  $\text{LaNiO}_3$ ; top electrode, Pt; bottom electrode,  $\text{SrRuO}_3$ .

Q10

1 tunnelling (FIT)<sup>22</sup>. By allowing only elastic electron tunnelling (that  
2 is, no thermal activation) between metallic junctions, which are  
3 subject to a small junction voltage fluctuation (the Johnson noise)  
4 of the order of  $(kT/C_{\text{junction}})^{1/2}$ , the model predicts a gradual  
5 decrease of  $R$  with  $T$  that is absent in the models for conventional  
6 metals. The fitted  $C_{\text{junction}}$  from Fig. 5b gives the junction geometry:  
7 as  $R$  decreases with further resetting, the junction gap narrows, sig-  
8 nalling that the choked nanometallic path gradually recovers. Such  
9 choked nanometallic paths are reminiscent of broken metallic fila-  
10 ments in conventional resistance memories<sup>9–16</sup>, although they can  
11 be electronically cleared by electron detrapping without atomic/  
12 ionic motion. Finally, with more electrons trapped and the nanome-  
13 tallic paths heavily choked, we also observed higher HR values  
14 with an insulator-like steep  $T$  dependence (one example is marked  
15 by \* in Fig. 5b). The intermediate and HR states therefore broadly  
16 encompass a spectrum of behaviour from bad metals to insulators,  
17 depending on the population of trapped electrons and film thick-  
18 ness. Further analysis is provided in Supplementary Fig. S8, which  
19 draws an analogy to other bad metals such as conducting  
20 polymers<sup>23</sup>.

21 The nanometallicity described here for random materials has a  
22 tunable carrier density and localization length  $\zeta$ . With conducting  
23 polymers as an outstanding example<sup>23</sup>, we suggest that nanometal-  
24 licity could be engineered by intimate mixing, at the atomic level, of  
25 other conducting and insulating components, which may be crystal-  
26 line or amorphous, including organic, biological and synthetic  
27 hybrid materials. These materials may have unusual, advantageous  
28 device characteristics. For example, by slightly reducing their

thickness, cells with the exponential  $R(\delta)$  dependence can lower  
the resistance by orders of magnitude to counter the resistance  
increase due to smaller cell areas. These new materials could also  
have disparate properties that are otherwise incompatible in conven-  
tional materials. Combining length-dependent (and anisotropic if  
sizes are disparate in different directions) nanometallicity with  
low thermal conductivity (for example, of  $\text{SiO}_2$ ) and high permittiv-  
ity (for example, of  $\text{HfO}_2$ ), properties that are of special interest to  
certain nanostructures<sup>24–26</sup> could be especially intriguing.

## Methods

Amorphous  $\text{SiO}_2$ :Pt and  $\text{Si}_3\text{N}_4$ :Pt films were deposited by radiofrequency co-  
sputtering using targets of Pt,  $\text{SiO}_2$  and  $\text{Si}_3\text{N}_4$  onto unheated single-crystal Si  
substrates (110 and 100 orientations) with a pre-deposited polycrystalline SRO  
electrode. Epitaxial perovskite films were grown on (001)  $\text{SrTiO}_3$  single-crystal  
substrates using pulsed laser ablation, with a SRO bottom electrode, at various  
temperatures. Substrates of (011) and (111)  $\text{SrTiO}_3$  were also used to vary the growth  
strain and verify the generality of the observations. Top electrodes were deposited by  
sputtering (Pt, Mo, Ta) or thermal evaporation (Au, Ag) through a shadow mask  
with various openings (typically 80  $\mu\text{m}$  in diameter) to define test cells. For  $\text{SiO}_2$ :Pt,  
Pt, Mo and Ta were also used as bottom electrodes. The high-resolution cross-  
sectional images of perovskites were taken with a JEOL 2010 LaB<sub>6</sub> transmission  
electron microscope operating at 200 kV. The plan-view transmission electron  
micrographs and diffraction of  $\text{SiO}_2$ :Pt showing its amorphous structure<sup>27</sup> were  
taken using films sputter-deposited onto carbon-coated microscopy (copper) grids.  
Optical reflectivity and transmittance were collected using  $\text{SiO}_2$ :Pt films deposited  
onto either fused silica substrates for UV-Vis measurements (Cary 5000  
spectrometer from Varian) or KBr substrates for IR measurements (Nicolet 8700  
FTIR from Thermo Scientific.) Impedance (d.c. and a.c.) was measured in air using a  
probe station, and also for UV irradiation (continuous energy of  $\sim 2.8$ – $4.1$  eV)  
experiments. Additional measurements (including four-point probing of sheet  
resistance) were conducted in various cryostats, in vacuum, using lithographically or  
shadow-mask defined cells of various sizes. In fitting the reflectivity data of Fig. 1b,  
the free electron contribution to reflectivity of Fig. 1b was fitted using Drude's  
formula for dielectric constant,  $\epsilon = 1 - \omega_p^2 / (\omega(\omega + i/\tau))$ , to find the plasma  
frequency  $\omega_p$  and carrier concentration ( $\propto \omega_p^2$ ). In fitting the data of Fig. 5b,  
Sheng's equation for tunnelling conductance,  $G = 1/R = G_0 \exp(-T_1/(T + T_0))$ ,  
was used to find  $T_1$  and  $T_0$ , from which the geometric parameters of the  
nanojunctions were obtained. Further details of the methods and the material  
characterization are provided in the following sections.

Received 24 September 2010; accepted 28 January 2011;

published online XX XX 2011

## References

- Mott, N. F. & Davis, E. *Electronic Processes in Non-Crystalline Materials* 2nd edn (Clarendon Press, 1979).
- Mott, N. F. Electrons in disordered structures. *Adv. Phys.* **16**, 49–144 (1967).
- Anderson, P. W. Absence of diffusion in certain random lattices. *Phys. Rev.* **109**, 1492–1507 (1958).
- Dynes, R. C. & Lee, P. A. Localization, interactions, and the metal–insulator transition. *Science* **233**, 355–360 (1984).
- Lee, P. A. & Ramakrishnan, T. V. Disordered electronic systems. *Rev. Mod. Phys.* **57**, 287–337 (1985).
- Shklovskii, B. I. & Efros, A. L. *Electronic Properties of Doped Semiconductors* (Springer-Verlag, 1984).
- Ghosh, S. K. & Pal, T. Interparticle coupling effect on the surface plasmon resonance of gold nanoparticles: from theory to applications. *Chem. Rev.* **107**, 4797–4862 (2007).
- Gravais, F. Optical conductivity of oxides. *Mater. Sci. Eng.* **R39**, 29–92 (2002).
- Waser, R., Dittmann, R., Staikov, G. & Szot, K. Redox-based resistive switching memories—nanoionic mechanisms, prospects, and challenges. *Adv. Mater.* **21**, 1632–2663 (2009).
- Szot, K., Speier, W., Bihlmayer, G. & Waser, R. Switching the electrical resistance of individual dislocations in single-crystalline  $\text{SrTiO}_3$ . *Nature Mater.* **5**, 312–320 (2006).
- Snider, G. S., Stewart, D. R. & Williams, R. S. The missing memristor found. *Nature* **431**, 80–83 (2008).
- Rossel, C., Meijer, G. I., Bremaud, D. & Widmer, D. Electrical current distribution across a metal–insulator–metal structure during bistable switching. *J. Appl. Phys.* **90**, 2892–2898 (2001).
- Sawa, A., Fujii, T., Kawasaki, M. & Tokura, Y. Hysteretic current–voltage characteristics and resistance switching at a rectifying  $\text{Ti}/\text{Pr}_{0.7}\text{Ca}_{0.3}\text{MnO}_3$  interface. *Appl. Phys. Lett.* **85**, 4073–4075 (2004).
- Kwon, D.-H. *et al.* Atomic structure of conducting nanofilaments in  $\text{TiO}_2$  resistive switching memory. *Nature Nanotech.* **5**, 148–153 (2010).

15. Wu, J. & McCreery, R. L. Solid-state electrochemistry in molecule/TiO<sub>2</sub> molecular heterojunctions as the basis of the TiO<sub>2</sub> 'memristor'. *J. Electrochem. Soc.* **156**, P29–P37 (2009).
16. Liu, C.-Y. & Hsu, J.-M. Effect of ultraviolet illumination on resistive switching properties of Cu<sub>x</sub>O thin film. *Jpn J. Appl. Phys.* **49**, 084202 (2010).
17. Kim, S. G., Wang, Y.-D. & Chen, I.-W. Strain relaxation in buried SrRuO<sub>3</sub> layer in (Ca<sub>1-x</sub>Sr<sub>x</sub>)(Zr<sub>1-x</sub>Ru<sub>x</sub>)O<sub>3</sub>/SrRuO<sub>3</sub>/SrTiO<sub>3</sub> system. *Appl. Phys. Lett.* **89**, 031905 (2006).
18. Wang, Y.-D., Kim, S. G. & Chen, I.-W. Strain relaxation in tensile and compressive oxide thin films. *Acta Materialia* **56**, 5312–5321 (2008).
19. Mamchik, A. & Chen, I.-W. Magnetic impurities in conducting oxides: I. (Sr<sub>1-x</sub>La<sub>x</sub>)(Ru<sub>1-x</sub>Fe<sub>x</sub>)O<sub>3</sub> system. *Phys. Rev. B* **70**, 104409 (2004).
20. Allen, P. B. *et al.* Transport properties, thermodynamic properties, and electronic structure of SrRuO<sub>3</sub>. *Phys. Rev. B* **53**, 4393–4398 (1996).
21. Lenzling, M. & Snow, E.-H. Fowler–Nordheim tunneling into thermally grown SiO<sub>2</sub>. *J. Appl. Phys.* **40**, 278–283 (1969).
22. Sheng, P. Fluctuation-induced tunneling conduction in disordered materials. *Phys. Rev. B* **21**, 2180–2195 (1980).
23. Menon, R., Yoon, C. O., Moses, D., Heeger, A. J. & Cao, Y. Transport in polyaniline near the critical regime of the metal–insulator transition. *Phys. Rev. B* **48**, 17685–17694 (1993).
24. Ohta, H. *et al.* Giant thermoelectric Seebeck coefficient of two-dimensional electron gas in SrTiO<sub>3</sub>. *Nature Mater.* **6**, 129–134 (2007).
25. Ozbay, E. Merging photonics and electrons at nanoscale dimensions. *Science* **311**, 189–193 (2006).
26. Engheta, N. Circuits with light at nanoscales: optical nanocircuits inspired by metamaterials. *Science* **317**, 1698–1702 (2007).
27. Bagley, B. G. & Turnbull, D. The preparation and crystallization behaviour of amorphous nickel–phosphorus thin films. *Acta Metallurgica* **18**, 857–862 (1970).

### Acknowledgements

This work was supported by the National Science Foundation (grant nos DMR-05-20020, 07-05054 and 09-07523). For the TEM analysis, we are grateful to K.C. Hsieh and Y. Lu at the Frederick Seitz Materials Research Laboratory (University of Illinois), partially supported by the US Department of Energy (grants DE-FG02-07ER46453 and DE-FG02-07ER46471).

### Author contributions

I.-W.C. conceived and designed the experiments and wrote the paper. A.B.C. performed the SiO<sub>2</sub>:Pt and SiN:Pt experiments. S.G.K. and Y.D.W. performed the perovskite experiments. W.S.T. performed the optical experiments. All authors analysed the data, discussed the results and commented on the manuscript.

### Additional information

The authors declare no competing financial interests. Supplementary information accompanies this paper at [www.nature.com/naturenanotechnology](http://www.nature.com/naturenanotechnology). Reprints and permission information is available online at <http://npg.nature.com/reprintsandpermissions/>. Correspondence and requests for materials should be addressed to I.W.C.

Publisher: Nature

Journal: Nature Nanotechnology

Article number nnano.2011.21

Author (s): Albert B. K. Chen *et al.*

Title of paper: A size-dependent nanoscale metal–insulator transition in random materials

Query no.	Query	Response
1	Sentence beginning “Our first example” OK as amended?	
2	We have separated and renumbered the two references in ref 15. Please check that subsequent renumbering is correct.	
3	Please check sentence beginning “One was”. I am not sure what you were referring to by “the other”. Do you mean the perovskite? Can we say “One was a Si <sub>3</sub> N <sub>4</sub> glass similarly doped with Pt; the other, which adopted a lattice construct that was perfectly regular but randomized by atomic mixing, was a perovskite solid solution made into an epitaxial thin film to avoid line and planar defects that might have provided electrical shorts <sup>17,18</sup> .”	
4	Changed to “application of a voltage” – OK?	
5	RF expanded OK?	
6	Changed to the proportional symbol – OK?	
7	There are no following sections – please check.	
8	Ref 9 – please check page range.	
9	What does the “c” represent in Fig 2b?	
10	Please check that the versions of Fig. 2 and 5a we have used are correct.	
11	Is there something missing after “100” here?	